

# Effect of Feedstock Powder on the Cold Sprayed Titanium Dioxide Coating

H. Hajipour<sup>a</sup>, A. Abdollah-Zadeh<sup>a,\*</sup>, H. Assadi<sup>b</sup>, E. Taheri Nasaj<sup>a</sup>, H. Jahed<sup>c</sup>

a. Department of Materials Engineering, Tarbiat Modares University, Tehran, Iran.

b. Brunel University London, Brunel Centre for Advanced Solidification Technology (BCAST), Uxbridge, United Kingdom

c. Mechanical and Mechatronics Engineering Department, University of Waterloo, Waterloo, Canada

Corresponding Author's E-mail: Zadeh@modares.ac.ir

## Abstract

The properties of cold-sprayed ceramic coatings depend not only on the process parameters but also on the feedstock powder characteristics. To clarify the effect of feedstock powder on cold spraying, two titanium oxide powders were used in this study: (1) nanopowder and (2) agglomerated powder prepared with nanoparticles and polyvinyl alcohol. The cross sections of the deposited coatings were observed by scanning electron microscopy (SEM). The results showed that the agglomerated powder with micrometer particles made of nano-sized particles passes successfully through the bow shock layer and reached the substrate, thus forming a coating. These particles are embedded into the substrate and form a strong interfacial coating/substrate bond. SEM images revealed that the metallic substrate undergoes plastic deformation, providing interlocking with the particles of the powder, and hence, reasonable bonding to the substrate.

**Keywords:** agglomerated powder, cold spray, nanopowder, powder particle morphology, TiO<sub>2</sub> coating

## 1. Introduction

The cold spray (CS) process, also known as cold gas dynamic spray, is a relatively new solid-state coating technique based on the high-speed impact of metals and ceramic particles on different substrates at low temperature. Unlike those in conventional thermal spray techniques, process gas temperatures are low enough and exposures to the hot gas stream are short enough to avoid melting of the particles [1-3]. CS method can be considered a safe and green technology because of the absence of a high-temperature explosive gases and radiation. Currently it's being used also as an additive manufacturing process for geometrical and/or structural restoration of defected parts [V.

Champagne & D. Helfrich (2015) Critical Assessment 11: Structural repairs by cold spray, *Materials Science and Technology*, 31:6, 627-634].

The higher particle velocity and lower processing temperature in CS produce a series of advantages compared to other coating techniques like thermal spray, sol-gel, sputtering, etc. The oxidation, grain growth and phase transformation can be avoided because there are limited heat effects on substrates and spray powders. Therefore, it is possible to deposit phase-transformation-sensitive materials, oxidation-sensitive materials and use an expanded range of substrates such as ceramics, metals and polymers [4]. In addition, the resulting residual stresses are normally relatively low and mostly compressive compared to those in thermal spray, which permits the deposition of thick coatings. CS is economical, having high deposition efficiency, a high deposition rate, and no need for a high temperature heat source. Another advantage is that the substrate needs no surface preparation to achieve good deposition. During the initial deposition stage, due to the high kinetic energy of the powder in the spray process, the particles impacting the substrate will act as cleaning agents in a way similar to sand-blasting. Surface contaminants such as dirt, oils and native oxide layers are removed by the initial particle collisions [5-6].

In the last decade much work has been done to explore the bonding mechanism during the CS process. The accepted hypothesis on the bonding process is that a coating is formed through the intensive plastic deformation of particles impacting a substrate at a temperature well below the melting point of the spray material. The bonding of cold-sprayed particles is associated with adiabatic shear instability, leading to large plastic strains, and occurs beyond a certain velocity [5]. At impact velocities above the critical velocity, a large proportion of the impact energy is converted to heat. Therefore, the temperature in the contact area rises rapidly which leads to viscoplastic material flow away from the impact site [7]. This jet cleans the oxide film off particles and substrate surfaces, increasing their activity for metallurgical bonding.

The CS process is most typically applied to metallic powder but not to ceramic ones because of their brittle characteristic [8]. A brittle ceramic would not go through plastic deformation, but would instead break. However, several studies have shown the ability to fabricate a ceramic coating such as TiO<sub>2</sub>, by cold spray. There is a specific interest in the deposition of TiO<sub>2</sub> coating by CS, as this technology would overcome the undesirable anatase to rutile phase transformation issues of TiO<sub>2</sub> coating. In 2004, Ballhorn et al. [9] initially reported on using CS to embed anatase particles in a plastic surface. The particles penetrated the polymer and provided a certain area of

metal oxide on the surface, which was intended to enable the photocatalytic degradation of contaminants. Later, in 2007, Klassen and Kliemann [10] used TiO<sub>2</sub> powder mixed with a ductile metallic powder to manufacture a photocatalytic coating by cold spray process. With this mixture, only 30-80% of metal oxide particles appear on the top surface of the coating, which may limit the final performance of the photocatalyst. After that, Kliemann et al. [11] investigated the formation of TiO<sub>2</sub> coatings on four different metal substrate types. The TiO<sub>2</sub> particles ranged from about 3 to 50 µm and was cold-sprayed using nitrogen as a processing gas with an inlet pressure of 4.0 MPa. The spray particles did not build up a coating because of their brittleness and the high pressure of the coating process. Due to fracture under the elastic rebound forces, the brittle sprayed particles broke, and only small remnants remained on the substrate. As a result, the researchers were unable to fabricate uniform TiO<sub>2</sub> ceramic coating by means of cold spray process.

In 2010, Yamada et al. [12] reported successful titanium oxide film production by cold gas spraying, and also showed that no modification to the cold spray equipment was needed. During the spraying, they changed process parameters such as the nature of the gas, the pressure and the temperature in order to understand whether they were important in fabricating TiO<sub>2</sub> ceramic coating. This study showed that the process gas conditions are not a main factor in ceramic deposition cold spray process. Furthermore, their results prove that the microstructural and mechanical characteristics of feedstock powder are the key influencers of the deposition efficiency and properties of cold spray coating. However, the influence of starting powder as an important parameter for the formation of oxide material coating by CS is not yet well understood.

In the present study, two types of TiO<sub>2</sub> powder, nano-crystal powder and submicron sized sintered powder, were used as feedstocks in the deposition of nanostructured TiO<sub>2</sub> coating on Aluminium substrate by cold spraying using nitrogen as the processing gas. The effect of the feedstock structure on the feasibility of coating fabrication was investigated. The morphology, and crystal structure of the powders and the microstructure of the coated sample were analyzed. In addition, some mechanical properties of the obtained coatings, including adhesion strength, hardness distribution were evaluated.

## **2. Experimental Procedure**

### **2.1. Materials**

Two types of commercially available TiO<sub>2</sub> powder (Cosmo chemical, Korea) were used as the starting powder in the present study. Powder A was composed of nanocrystal particles and powder B was prepared through agglomerating ultra-fine particles, using polyvinyl alcohol as a binder. The agglomerate powder was tempered for 2 h at 800 °C in air atmosphere before spraying. An aluminium plate with dimensions of 100 mm × 30 mm × 1.5 mm was employed as a substrate for film deposition. An average Vickers microhardness of 47.97 ± 1.2 HV was obtained for the substrate under a 100 gram load. Prior to spraying, the substrate was rinsed with acetone. The chemical composition of the substrate was measured by energy dispersive X-ray (EDX) spectroscopy and is presented in Table 1.

Table 1 Chemical composition of Aluminum substrate

Weight %	Al	Si	Mg	Fe	Zn	Cu	Mn
substrate	Balance	1.79	0.5	0.41	0.38	0.26	0.09

## 2.2. Processing of coating

A custom built high pressure cold spraying system was employed to deposit the coating. A spray gun with a converging-diverging de Laval-type nozzle with a throat diameter of 2 mm was adopted. The substrate was moved by an X-Y drive system at a traverse speed of 20 mm/s during spraying in order to form a uniform-thickness coating. Nitrogen gas was employed as both an accelerating gas and powder feeding gas, at a pressure of 15 and 16 bar, respectively. The gas temperature in the prechamber was 500 °C. The standoff distance from the nozzle exit to the substrate surface was 35 mm.

## 2.3. Powders and coating characterization

X-ray diffraction was used to detect the phase and crystalline structure of the powders. XRD patterns were obtained using a Co- $\alpha$  radiation ( $\lambda = 1.78897 \text{ \AA}$ ) source at a setting of 40 mA and 40 kV (X'Pert MPD, Philips, Holland). XRD Spectra were recorded by scanning  $2\theta$  in the range 10-90°. The average crystallite size of the TiO<sub>2</sub> powders were estimated using the XRD data and the Scherrer equation (1) below:

$$D = \frac{K \lambda}{\beta \cos\theta} \quad (1)$$

where  $D$  is the crystallite size in nm,  $k$  is the shape constant (0.9),  $\lambda$  is the X-ray wavelength of Co- $\alpha$  radiation in nm,  $\theta$  is the Bragg's angle in degrees, and  $\beta$  is the observed peak width at half-maximum peak height in rad. The coated samples were prepared using cold mounting, grinding and fine polishing to achieve the desired surface. The powder morphology and cross section microstructure of the granule powder and coating were observed by scanning electron microscope (SEM: Philips XL30) and field emission scanning electron microscopy (FESEM: MIRA3 TESCAN). The porosity of the granule powder and coating was determined using image processing from the cross sectional SEM images. The surface roughness of the substrate before and after spraying was determined by field emission scanning electron microscope cross section image. The microhardness of powder B was tested with a microhardness tester under a 100 g load for a loading time of 10 s, while the microhardness of the substrate was tested under a 100 g load for a loading time of 20 s. Mechanical properties of the coating were measured with nano indentation using a Triboindenter (Hysitron Inc., Minneapolis, USA). Nano indentation testing was performed with a new Berkovich tip (~50 nm tip radius) with loading conditions of 1mN maximum indentation load, and 200  $\mu$ N/s loading and unloading rates. The adhesion between the coating and the Al substrate was evaluated by ultrasonic cleanout. Coatings were put in a 185 W ultrasonic cleaner for 1 min. The adhesion was evaluated according to the spalling state of the coating.

### 3. Results and Discussion

#### 3.1. Characterization of feedstock powder

XRD spectra of the starting powders are shown in Fig. 1. It can be seen that powder A has a single phase anatase structure and powder B has both anatase and rutile phase structures. The existence of the rutile phase is due to the annealing process at 800 °C. The rutile content in powder B was calculated by using the diffraction intensity of rutile and anatase in the XRD pattern. The following equation was used to estimate the rutile content in powder B.

$$X_R = \frac{1}{1 + 0.8 (I_A/I_R)} \quad (2)$$

where  $X_R$  is the rutile content in powder B, and  $I_A$  and  $I_R$  are the intensity of the anatase peak (101) and rutile peak (110), respectively, in the XRD pattern. Powder B was composed of 97.34% anatase phase and 2.66% rutile phase. It is obvious that the dominant crystal phase present in powder B after heat treatment is an anatase phase with tetragonal crystal structure. The crystallite sizes calculated using the Scherrer's equation were 34 and 40 nm for powders A and B, respectively. Heat treatment increases the crystallite sizes and crystallinity in  $\text{TiO}_2$  powder.

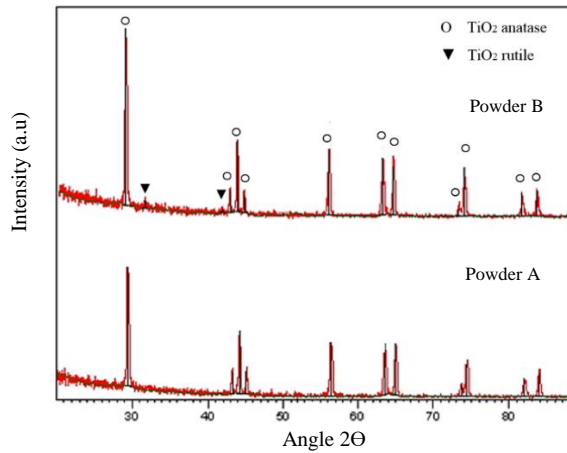


Fig. 1 The XRD spectra of feedstock powders.

The morphology and the size distribution of the powders A and B used as coating materials are shown in Fig. 2 and 3, respectively. The average particle sizes of the powders were measured from SEM images. Fig. 2 reveals that powder A consists of spherical ultra-fine particles with a diameter of about  $100 \pm 15.3$  nm. Fig. 3 displays that powder B has a dense agglomerated structure consisting of very fine nano particles. The morphology of powder B is spherical, with a diameter of about  $80 \pm 11$   $\mu\text{m}$ .

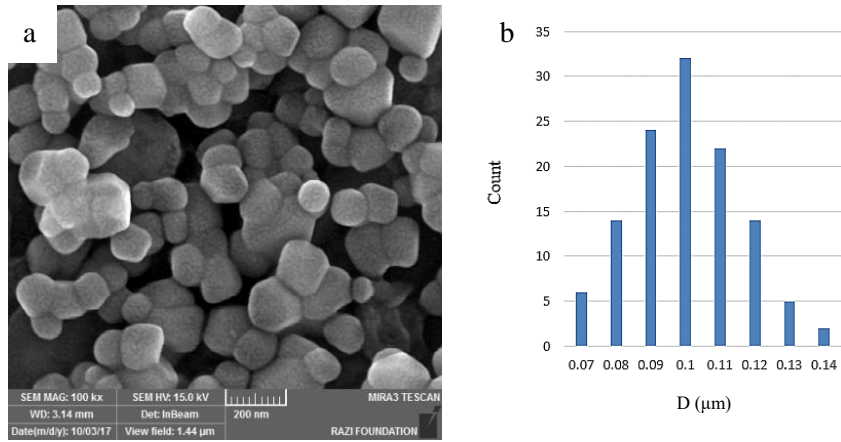


Fig. 2 Powder A characterization: (a) morphology of TiO<sub>2</sub> powder, (b) particle size distribution.

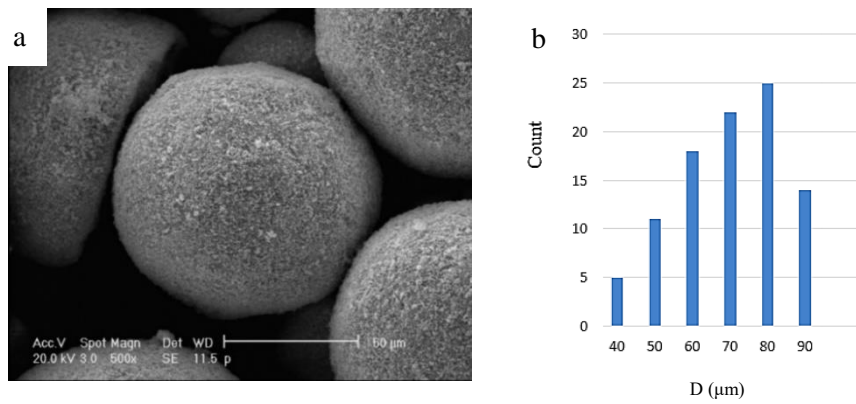


Fig. 3 Powder B characterization: (a) SEM micrograph, (b) particle size distribution.

Figure 4 shows the cross-sectional SEM image of powder B. Nearly all particles in powder B exhibited a spherical morphology and porous microstructure. The measurement results showed that the powder's porosity is  $21 \pm 0.8$ , and its microhardness is  $17.5 \pm 2.2 \text{ HV}_{0.1}$ .

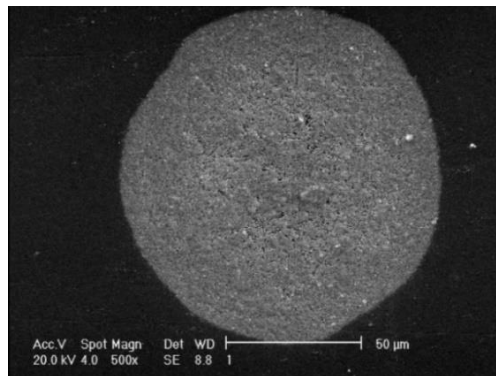


Fig. 4 Cross-sectional view of the powder B.

### 3.2. Characterization of coating

Fig. 5 shows a cross section of cold-sprayed  $\text{TiO}_2$  coating deposited on Aluminium substrate with powder A. It is clear that only a very thin coating is present on the substrate surface. The thickness of the coating is about 490 nm, and it was found that the coating thickness could not build up further due to starting powder characteristics. Powder A consists of fine nano particles that have a loosely agglomerated morphology. This uncontrolled agglomeration of nanoparticles is due to their high surface energy. Few of the spherical nano particles and irregular loose agglomerate particles can cross through the bow shock layer near the substrate, due to their small size. Therefore, it seems that only around 10 – 20 % of powder A was deposited on the substrate since a thicker ceramic coating did not build up.

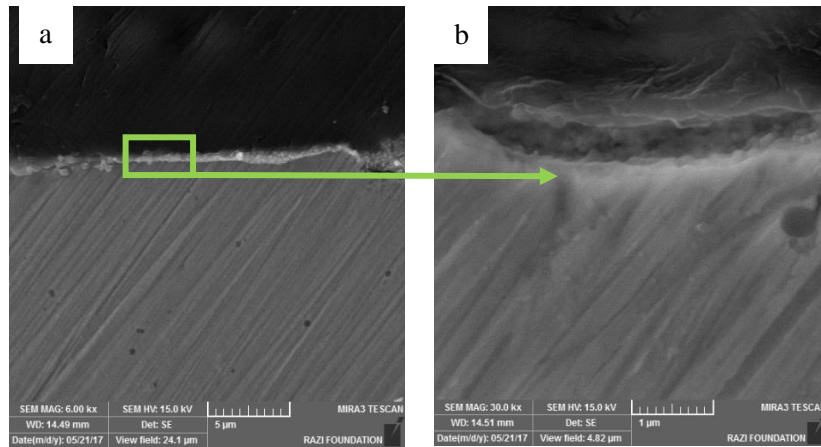


Fig. 5 FESEM micrograph of the  $\text{TiO}_2$  coating deposited with powder A: (a) cross-sectional image, (b) zoom up image.

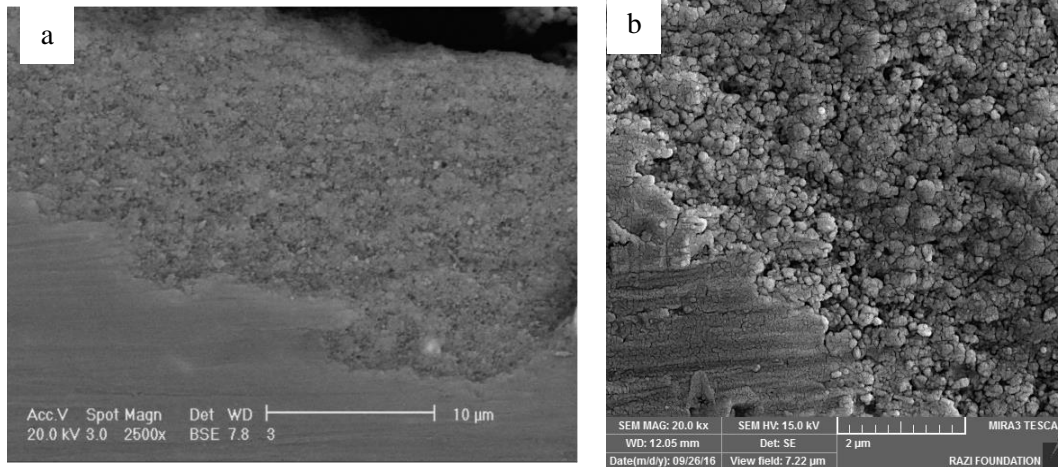


Fig. 6 Interface between the TiO<sub>2</sub> coating by powder B and Al substrate: (a) SEM images of cold-sprayed TiO<sub>2</sub> coating, (b) FESEM of Interface.

Figure 6 shows the cross-sectional microstructure of the coating prepared with powder B. It is clear that continuous TiO<sub>2</sub> coating with a thickness of 10–15 μm was deposited on the substrate surface. In comparison to Fig. 5, powder B formed a more-defined and thicker coating. Detailed observation of the interface between coating and substrate shows no delamination, and good adhesion. Most of the impacted particles stick to each other well and build up the coating. Although it is impossible for ceramic particles to deform under the impact of spray particles, the tamping effect will compact particles under high impact pressure. As a result, an apparently dense coating is formed with the successive deposition of spray particles.

It seems that both powder types were deposited under the same conditions, and there are no visible large pores and cracks, due to the tamping effect caused by the continuous impacts of particles. Apart from these similarities, the thickness of the coatings achieved with powders A and B differ, as shown in Fig. 5 and 6. That with powder B is 20-30 times thicker than that with powder A. Since the coating deposition parameters are same for both coatings, it seems that the starting-powder characteristics caused this difference.

The differences between powders A and B during the cold spray process are explained next. As shown in Figs 2 and 3, the particle size distributions of the two powders differ significantly, in turn significantly affecting the flow ability of the powders. As an example of the latter, powders typically exhibit poorer flow properties than coarse particles or agglomerates. These agglomeration can be a valuable tool in improving the flow ability of powders. In cold spraying,

it is very difficult to feed small particles. Therefore, powder B can be carried with N<sub>2</sub> gas and reach the substrate more easily than powder A.

Studies have shown that particle velocity has a strong effect on coating deposition. To reveal differences during deposition of the two powder types, the particle velocity for each powder was calculated by the formula mentioned in Assadi et al.'s [13] paper. Their formula consider the effect of various factors on particle velocity:

$$V_{pi} = V \left( 1 + \frac{\rho_0 \delta}{\rho_p d_p} \right)^{-1} \quad (3)$$

where  $V_{pi}$  is the impact velocity of particles,  $\rho_0$  gas stagnation density,  $\delta$  is a fitting parameter of about 0.0007 m,  $\rho_p$  is particle density,  $d_p$  is particle diameter, and  $V$  is the approximated particle velocity at the nozzle exit, calculated as follows:

$$V = \left( \frac{c_2}{\sqrt{R T_0}} + \sqrt{\frac{\rho_p d_p}{C_d L_d \rho_0}} \right)^{-1} \quad (4)$$

where  $c_2$  is 0.42 for nitrogen,  $R$  is the universal gas constant,  $T_0$  is the gas stagnation temperature,  $C_d$  is the drag coefficient, and  $L_d$  is length of the diverging (supersonic) part of the nozzle. According to Eq. 3 and 4,  $V_{pi}$  is plotted as a function of particle sizes for powders A and B. Fig. 7 a and b show the variation of impact velocity versus particle sizes for powder A and B, respectively. It is clear that the particle impact velocity, in response to particle size, increases from 40 to 67 m/s for powder A and 480 to 600 m/s for powder B. For the average particle size of powder B, the average impact velocity is about 520 m/s, which is much higher than the impact velocity for powder A. In summary, powders with larger particles accelerate to a higher velocity and so are more easily deposited onto the substrate than the powders with smaller particle.

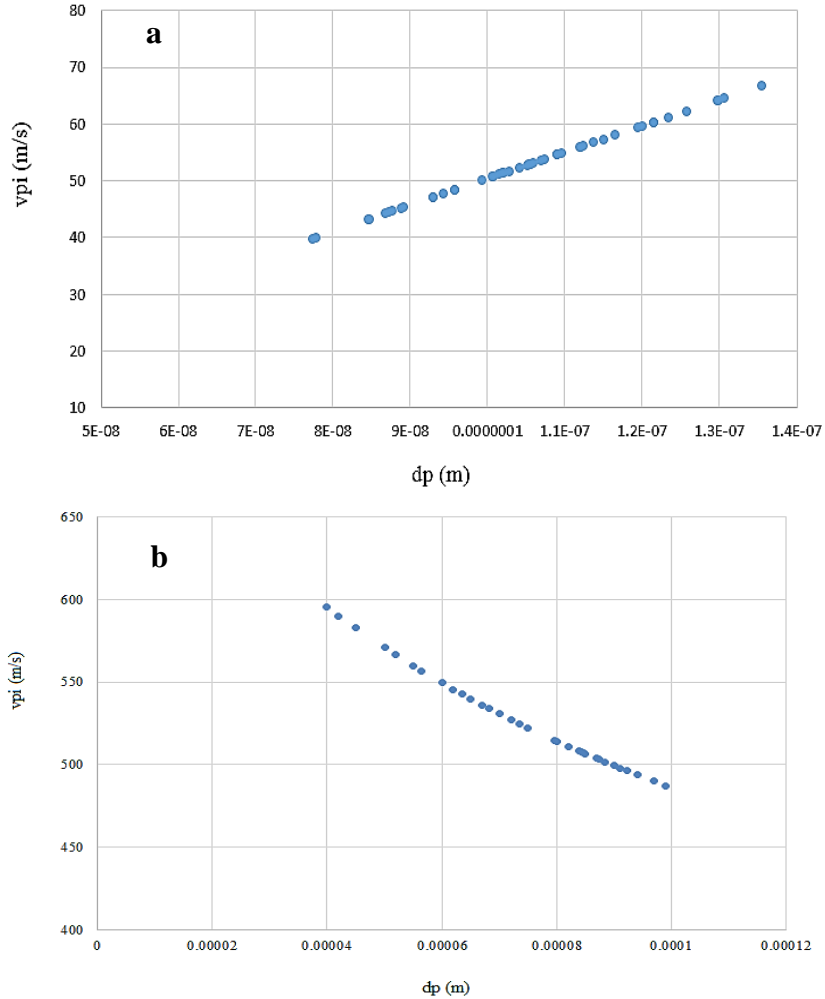


Fig. 7 Variation of the particle impact velocity for; (a) powder A, (b) powder B.

One of the important parameters that effect powder A spraying and its velocity is the bow shock layer. The bow shock has a negative influence on deposition efficiency as a result of reduced particle velocity. Powder A, due to its very small particles, has low kinetic energy and is significantly slowed by the bow shock layer. Therefore, in the CS process, powder A is deflected before it reaches the substrate. Gilmore et al. [14] and Hanft et al. [15] predicted that the smallest particles ( $< 5\text{--}15 \mu\text{m}$ ) could be decelerated and even deflected away from the substrate by the bow shock. In conclusion, powder B, because of its agglomerate structure, has better flow ability and can pass through the bow shock layer and hit the substrate at high speed, but powder A, with its very small nano particles, cannot reach to the substrate at an appropriate velocity.

Based on the discussion above, powder B obtains high kinetic energies and hits the substrate at high velocity, leading to plastic deformation of the metallic substrate, associated with increased surface roughness. As shown in Figs 8 and 9 the surface roughness increases significantly after cold spray deposition of powder B. This roughness causes mechanical entanglement that might also play an important role in the buildup stage [11]. For brittle materials like ceramics, the first layer is achieved by plastic deformation of the ductile metallic substrate; i.e., the particles are embedded into the substrate without any additional binding agent or calcination procedure. Fig. 9 (b) shows that the coating/substrate interface is relatively rough when the particles hit the substrate at a high speed. As a result, titanium oxide particles embed in the Al substrate. Although the deposition mechanism of CS has not been understood well until now, but it is clear that the powder structure and properties are crucial for the preparation of the desired coatings.

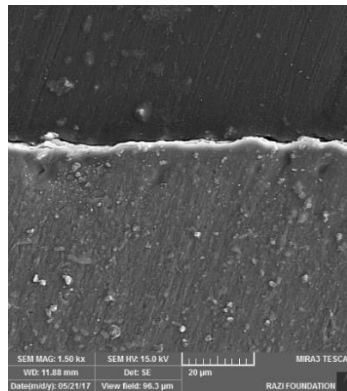


Fig. 8 Surface roughness of the Al substrate before coating.

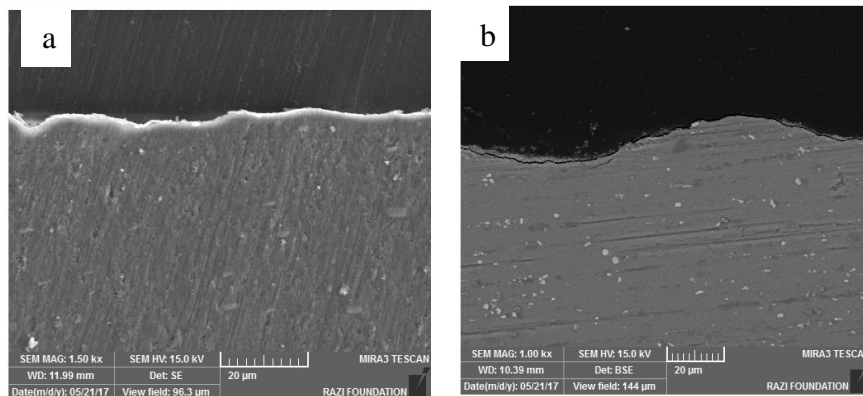


Fig. 9 Surface roughness of the Al substrate after cold spray process with; (a) powder A, (b) powder B.

The porosities of powder B and the TiO<sub>2</sub> coating were measured using cross sectional SEM images. Image analyzer results show these porosities as  $21.5 \pm 0.8$  and  $12.7 \pm 1.6$ , respectively. Compared to the initial powder, the coating has lower porosity. Subsequent impacts of other particles may have partly lessened the porosity of the coating by hammering the previously deposited particles into the substrate.

Fig. 10 (a) and (b) show the surface morphology of the coating before and after ultrasonic cleaning, respectively. For the coatings deposited with powder B, no spalling of the fabricated coating occurred to the sample. The coating shows good enough adhesion with the substrate as well as good cohesion within the coating. The boundaries between the particles become ambiguous in both the surface and cross section (Fig. 6a), suggesting that strong particle/ particle bonding occurred in the coating with powder B.

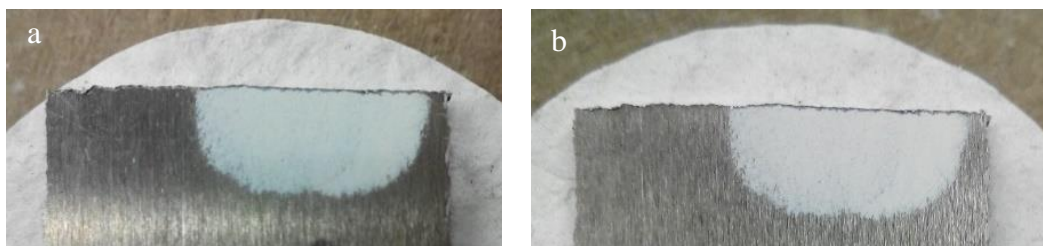


Fig. 10 Surface morphologies of the coatings by powder B (a) As-deposited layer, (b) after ultrasonic cleaning for 60 sec.

## Conclusion

Differences during the deposition of titanium oxide coating were investigated using two different powder types, nano TiO<sub>2</sub> powders and agglomerated powders. Better particle/substrate bonding and build-up continuous ceramic coating were observed for the agglomerate submicron powder. One of the important factors that causes this difference during cold spraying is particle velocity, which is affected by two competing mechanisms outside of the nozzle during CS: particle acceleration/deceleration due to the free gas jet and particle deceleration due to the presence of bow shock. Particle velocity may increase outside of the nozzle; however, the presence of the bow shock, which exists a short distance from the substrate, can theoretically reduce it. In this study, the agglomerate TiO<sub>2</sub> powders pass through the bow shock layer and impact the substrate at high

velocities. In this case the substrate is deformed due to high impact velocities of the agglomerate powders. In addition, the porosity of the TiO<sub>2</sub> agglomerate powder may lead to the breaking down of the particles when impacting the substrates. Then, the crystals are decoupled and their newly unstable surfaces bond to other counterparts, creating more stable interfaces, which allows for the bonding of the newly impacting particles and thus the build-up of the coating. In conclusion, through optimization of the powder structure, the properties of cold sprayed ceramic coating can be improved and tailored for better performance.

## Reference

- (1) Frank Gartner, Thorsten Stoltenhoff, Tobias Schmidt, and Heinrich Kreye, “The Cold Spray Process and Its Potential for Industrial Applications”, *Journal of Thermal Spray Technology*, Vol. 15, pp. 223- 232, 2006.
- (2) N. Bala, H. Singh, J. Karthikeyan, S. Prakash, “Cold spray coating process for corrosion protection: a review”, *Surf. Eng.*, Vol. 30, pp. 414–421, 2014.
- (3) S. Grigoriev, A. Okunkova, A. Sova, P. Bertrand, I. Smurov, “Cold spraying: From process fundamentals towards advanced applications”, *Surf. Coatings Technol.* Vol. 268, pp. 77–84, 2014.
- (4) S. Dosta, Giovanni Bolelli, Alessia Candeli, Luca Lusvarghi, Irene Garcia Cano, Josep Maria Guilemany, “Plastic deformation phenomena during cold spray impact of WC-Co particles onto metal substrates”, *Acta Materialia*, Vol. 124, pp. 173-181, 2017.
- (5) W. Li, H. Assadi, F. Gaertner, and Sh. Yin, “A Review of Advanced Composite and Nanostructured Coatings by Solid-State Cold Spraying Process”, *Critical reviews in solid state and materials sciences*, pp. 1–48, 2018.
- (6) S. Yin, X. F. Wang, X. K. Suo, H. L. Liao, Z. W. Guo, W. Y. Li, and C. Coddet, “Deposition behavior of thermally softened copper particles in cold spraying”, *Acta Mater*, Vol. 61, pp. 5105–5118, 2013.
- (7) K. Kim, M. Watanabe, and S. Kuroda, Bonding Mechanisms of Thermally Softened Metallic Powder Particles and Substrates Impacted at High Velocity, *Surf. Coat. Technol.*, Vol. 204, pp. 2175-2180, 2010.

- (8) A. Moridi<sup>1</sup>, S. M. Hassani-Gangaraj, M. Guagliano and M. Dao, “Cold spray coating: review of material systems and future perspectives”, *Surface Engineering*, VOL 36, pp. 369-395, 2014.
- (9) R. Ballhorn, F. Peterka, H. Kreye, I. Burlacov, T. Stoltenhoff, and J. Jirkovsky, “Production of Photocatalytically Active Polymer Surfaces of Variable Composition Comprises Cold Gas Spraying them with Oxide Powder to Produce Adherent Photocatalytic Layer”, German Patent Number: DE102004038795A1, 2004.
- (10) T. Klassen and J.A. Kliemann, “Method for manufacturing a photocatalytically active layer”, United States Patent US2007148363A1, 2007.
- (11) J.O. Kliemann, H. Gutzmann, F. Gartner, H. Hubner, C. Borchers, and T. Klassen, “Formation of Cold-Sprayed Ceramic Titanium Dioxide Layers on Metal Surfaces”, *Journal of Thermal Spray Technology*, Vol. 20, pp. 292- 298, 2011.
- (12) M. Yamada, H. Isago, H. Nakano, and M. Fukumoto, “Cold Spraying of TiO<sub>2</sub> Photocatalyst Coating With Nitrogen Process Gas”, *Journal of Thermal Spray Technology*, Vol. 19, pp. 1218-1223, 2010.
- (13) H. Assadi, T. Schmidt, H. Richter, J.O. Kliemann, K. Binder, F. Gartner, T. Klassen, and H. Kreye, “On Parameter Selection in Cold Spraying”, *Journal of Thermal Spray Technology*, Vol. 20, pp. 1161- 1176, 2011.
- (14) D. L. Gilmore, R. C. Dykhuizen, R. A. Neiser, M. F. Smith, T. J. Roemer, “Particle velocity and deposition efficiency in the cold spray process”, *Journal of Thermal Spray Technology*, Vol. 8, pp 576–582, 1999.
- (15) D. Hanft, J. Exner, M. Schubert, T. Stöcker, P. Fuierer and R. Moos, “An Overview of the Aerosol Deposition Method: Process Fundamentals and New Trends in Materials Applications”, *Journal of Ceramic Science and Technology*, Vol. 6, pp. 147-182, 2015.